Published in final edited form as:
J Comp Neurol. 2008 November 20; 511(3): 360–372. doi:10.1002/cne.21847.

Altered olfactory epithelial structure and function in feline models of mucopolysaccharidoses I and VI

Fritz W. Lischka[1], **George Gomez**[2], **Karen K. Yee**[1], **Luba Dankulich-Nagrudny**[1], **Leen Lo**[1], **Mark E. Haskins**[3], and **Nancy E. Rawson**[1]

[1] Monell Chemical Senses Center, Philadelphia, PA, 19104-3308, USA

[2] Department of Biology, University of Scranton, Scranton, PA, 18510-4625, USA

[3] School of Veterinary Medicine, University of Pennsylvania, Philadelphia, PA, 19104-6051, USA

Abstract

The mucopolysaccharidoses (MPS) are a family of lysosomal storage diseases resulting in developmental defects and, in some types, mental retardation and other neurological symptoms. To gain insight into the neurological dysfunction in MPS, we examined the morphology of olfactory epithelia (OE) and physiology of olfactory receptor neurons (ORNs) in cat models of MPS I, a type in which neuronal lesions are prominent, and MPS VI, in which they are essentially absent. Histopathology showed that both groups of MPS-affected cats had significantly thinner olfactory epithelia than controls. While immature and mature ORNs were present in both MPS I and VI affected OE, the OE of MPS I-affected cats was structurally disorganized. ORN function was assessed with calcium imaging and patch-clamp recording. Few viable ORNs were recovered from MPS VI cats, but these exhibited normal responses to odors and pharmacological stimuli. In contrast, viable ORNs were as prevalent in MPS I as in controls, but were significantly less likely to respond to odor stimuli, although other responses were normal. Disrupted OE organization and impaired ORN function in MPS I, but not MPS VI, corresponds to the central nervous system (CNS) lesions found in MPS I but not MPS VI. These data represent the first neurophysiological correlate of this correspondence and have implications for understanding both the role of glycosaminoglycans in maintenance of the OE, as well as for targeting further research into the basis for and treatment of the neurological consequences of MPS disorders.

Keywords

receptors; nose; cell physiology; animal model; lysosomal storage; glycosaminoglycan

Introduction

The genetic mucopolysaccharidoses (MPS) are a family of lysosomal storage diseases resulting from partial catabolism of several glycosaminoglycans (GAGs). The enzyme deficiencies associated with MPS result in accumulation of partially degraded GAGs within lysosomes; defects in different enzymes result in related syndromes, grouped as MPS I through IX. In humans, clinical features include a variety of craniofacial, visual, and auditory impairment, and in some types, mental retardation. MPS I (alpha-L-iduronidase deficiency) and VI (arylsulfatase B deficiency) have been described in cats, and studies of

Corresponding author: Fritz W. Lischka, Monell Chemical Senses Center, 3500 Market Street, Philadelphia, PA 19104-3308, Telephone # (267) 519-4825, Fax # (267) 519-4701, e-mail: lischka@monell.org.

these animals have proven useful in understanding the disorders and in developing therapeutic approaches (Haskins et al., 1980; Haskins, 2007).

While a variety of neuroanatomical abnormalities of MPS-affected cats have been characterized, the neurophysiological and cellular changes underlying the neurological lesions are not clearly understood (Neufeld and Muenzer, 2001). Neuronal lesions are seen in MPS I and may impair integration and processing of neural activity (Walkley et al., 1988). Whether this abnormal morphology is the sole or initial cause of neurophysiological dysfunction in MPS I is unknown, and no prior studies have examined the impact of the MPS I enzyme defect on the functional characteristics of neurons. A better understanding of the neuropathology is needed to design adjunct therapeutic approaches to alleviate the neurocognitive impairment in children.

We examined this issue in an established animal model, the MPS-affected cat, in a neuronal system exhibiting an array of well-characterized neurophysiological and cellular characteristics, the olfactory system. Olfactory receptor neurons (ORNs) provide a useful tool to study neuropathology as they are easily obtained, have well-characterized cell signaling pathways that can be manipulated with known stimuli, and exhibit structural and functional properties similar to other CNS neurons (Schild and Restrepo, 1998). Functional properties of feline ORNs are generally similar to those of other species, with some features more comparable to those of humans than rodents (Gomez et al., 2005). In addition, human ORN's are accessible to biopsy procedures and can be extracted from patients without causing permanent damage, enabling studies of neuropathology in living subjects (Lovell et al., 1982; Hahn et al., 2005). Evidence also suggests that one the substrates of the alpha-L-iduronidase enzyme, heparan sulfate proteoglycans, play a role in the development and maintenance of the olfactory system (Tisay and Key, 1999;Toba et al., 2002), and possibly in the functional expression and trafficking of olfactory receptor proteins (Katada et al., 2004). Accordingly, we asked whether the structure and function of the olfactory epithelium were altered in cats affected with MPS I compared to normal and MPS VI cats that do not have CNS lesions. Our studies focused on: histological examination of the integrity of the olfactory epithelium, measuring stimulus-elicited odor responses in ORNs from MPS-affected cats, and electrophysiological characterization of voltage-activated ion channels. We show that the sensory epithelium is altered in both structure and function by MPS. In both MPS I and VI, the olfactory epithelium was thinner than normal, suggesting impairment in the ability of the OE to be repaired and maintained. MPS I was associated with a more severe neurophysiological dysfunction with a loss of responsiveness of the ORNs to odor stimulation, consistent with the occurrence of mental retardation as a sign of this disease in children. In contrast, MPS VI-affected cats exhibited abnormal OE structure, with fewer viable ORNs, but little functional impairment.

These findings suggest that the failure of the GAG-processing enzyme in MPS I leads to impairment at the level of the odorant receptor, or coupling to its associated G-protein, rather than to a general loss of neurogenesis, cellular function, or viability. As the more severe forms of MPS I are associated with neurological dysfunction, while MPS VI is not (Neufeld and Muenzer, 2001), these observations suggest that the selective functional defect underlying this neuropathology may relate to failure of G-protein-coupled receptors to properly insert into the neuronal cell membrane and/or to couple to their associated signaling pathways. Thus, these results hold implications both for understanding the molecular basis underlying the development of mental retardation in MPS disease as well as the molecular regulation of olfactory neuron development and replacement.

MATERIALS AND METHODS

Animals and tissue collection

Experiments described in this work conformed to the National Institutes of Health guide for the care and use of laboratory animals (NIH Publications 80–23, revised 1978), and efforts were made to minimize the number of animals used. Male and female cats aged 2 weeks to adult were used. Animals were housed with *ad libitum* food and water, 12-hour light cycles, at 21°C, with 12 – 15 air changes per hour. Feline olfactory tissue was obtained as described previously (Gomez et al. 2005) at autopsy from animals housed and euthanized for other studies of GAG storage disorders or for necessary colony management at the University of Pennsylvania, School of Veterinary Medicine in accordance with protocols approved by its Institutional Animal Care and Use Committee and the guidelines of the American Veterinary Medical Association. Affected and wild type (control) cats were identified by PCR and selected from among littermates when possible, or were age-matched with cats raised under identical conditions. A total of 57 animals were used for these studies: 15 for anatomical studies (see below) and 42 for calcium imaging and electrophysiological experiments (see Table 1).

For anatomical studies, the anterior portion of the head containing the nose and olfactory bulbs was removed and fixed in 4% paraformaldehyde in phosphate buffered saline (PBS) for 1 – 7 days. The heads were decalcified in Sorenson's solution (5% EDTA in phosphate buffer, pH = 6.8) and cryoprotected in sucrose series. Lower jaw and muscles were removed and the noses were frozen in M1 embedding matrix (Shandon Lipshaw, Pittsburgh, PA). The entire nose was cut at 16 – 20 μm coronal sections at various intervals. Every 5^{th} section was kept from tip of the nose to the beginning of the sensory epithelium, and then every other section was kept until the appearance of the olfactory bulbs, for which every 5^{th} section was kept. Sections were placed onto Superfrost Plus slides (Fisher Scientific) or Starfrost Adhesive slides (Mercedes Medical) and stored at −80°C. We analyzed OE sections from cats affected with MPS I (n=4; 7, 17, 25 and 88 weeks old), MPS VI (n=5; 24, 24, 27, 109 and 110 weeks old); and controls that were heterozygous for MPS I- or VI-affected genes or wildtype (controls; n=6; 5, 5, 17, 27, 72 and 288 weeks old).

Staining and Immunohistochemistry

Ten slides at intervals of 160 – 200 μm were selected from each cat, dried at 37°C, and stained with Alcian Blue pH=2.5 for 10 minutes (Fisher Scientific, Pittsburgh, PA USA) followed by Nuclear fast red (Vector Laboratories, Burlingame, CA, USA,) for 3–4 minutes for morphological studies. For immunohistochemistry, endogenous peroxidase and nonspecific binding were blocked by 0.3% hydrogen peroxide for 20 minutes and SuperBlock blocking buffer (#37517 Pierce, Rockford, IL USA) for 4 hours. Sections were incubated with antibody diluted in 10% SuperBlock overnight at 4°C in a humidified chamber followed by secondary biotinylated antibody and the avidin-biotinylated horseradish peroxidase complex (ABC Elite Kit, Vector Laboratories, Burlingame, CA). The sections were then incubated with Peroxidase Substrate Kit DAB, dehydrated and mounted with Permount (Fisher Scientific). Antibodies used included olfactory-specific and general neuronal markers.

Olfactory marker protein (OMP) is a polyclonal goat antiserum generated against OMP whole protein purified from rat (dilution 1:1000, generous gift of Dr. F. Margolis and purchased from Wako, Richmond, VA #544-10001). A western blot for this OMP antibody was performed using feline olfactory and brain tissue extracted and analyzed using standard protocols (Sambrook et al., 1989) and confirmed recognition of a single band of the predicted size (19kD, data not shown). This antibody is highly specific for mature olfactory

receptor neurons (Keller & Margolis, 1975) and selective staining is observed in a wide variety of species e.g., fish, rodent, and human (Buiakova et al., 1994; Ferrando et al. 2007).

Mouse monoclonal anti-neuronal class III β-tubulin (NST, dilution 1:500, Covance, Berkeley, CA #MMS-435P) was used to identify both mature and immature olfactory neurons. This antibody was raised against microtubules derived from rat brain and recognized the epitope CEAQGPK in the carboxyl-terminus of class III β-tubulin (TUJ1) (Lee et al., 1990a). On western blots of subtilisin digested purified rat brain, this antibody recognized only a single band of the predicted size for β-tubulin at 50kDa (Lee et al., 199b). This antibody has been characterized in olfactory receptor neurons of both embryonic and adult rats (Roskams et al., 1998) and humans (Ronnett et al., 2003).

We also assessed neuronal structures with an antibody for neural cell adhesion molecule (NCAM, dilution 1:1000, Sigma #C9672). This monoclonal mouse antibody (clone OB11) was generated from a fusion of mouse myeloma cells and splenocytes using embryonic rat brain growth cones as the immunogen (Neill et al., 1990). In P2 membrane fractions from whole rat and cat cortex, this antibody recognized only bands of predicted size of NCAM at 145kDa and 170kDa, the short and long cytoplasmic domains which arise from alternative splicing of NCAM mRNAs (Naegele and Barnstable, 1991).

To the best of our knowledge, none of these three antibodies have previously been characterized in the cat olfactory epithelium. The immunolabeling of only mature and/or immature olfactory receptor neurons and olfactory axonal bundles by these antibodies that we observed in the cat tissue was comparable to the labeling patterns observed in adult mouse olfactory epithelium (see Supplemental Fig 1).

Negative controls were done by substituting primary antibody with either ChromPure Goat IgG, whole molecule (Jackson ImmunoResearch Laboratories, Inc., West Grove, PA, #0005-000-003) or ChromPure Mouse IgG, whole molecule (Jackson ImmunoResearch Laboratories, #015-000-003) at similar concentrations to primary antibodies. Sections were stained and processed for each antibody simultaneously to control for variability. Photomicroscopy was carried out with a Nikon Microphot AF microscope attached to the Kodak Spot III digital camera and ImageProPlus software (MediaCybernetics). Digital images were cropped, arranged, and adjusted for contrast and white balance using PhotoshopCS v8 (Adobe Systems, Inc., San Jose, California).

Quantitative Analysis

The percent of goblet cell area and olfactory epithelial thickness were measured in the Alcian Blue/Nuclear Fast Red stained sections. For each cat, 10 sections containing both respiratory epithelium and olfactory sensory epithelium were chosen at a distance approximately 80 – 2400 μm apart depending on the age of the cat, determined to reflect comparable cross-sectional profiles. Along the septum, 10 regions along the left and 10 along the right respiratory epithelial surfaces were imaged with a 20X objective, representing an area of interest (AOI) of 600 μm × 425 μm. The area of the goblet cells and thickness of apical mucus layer were manually measured using ImagePro Plus software and calculated as percentage area of goblet cells/area of measured respiratory epithelium. The left and right sensory olfactory epithelium along the septum and ventral to the septal arch were imaged with a 10× objective, representing an AOI of 1200 μm × 855 μm, for measurements of epithelial thickness. Overall, twenty measurements of goblet cell density and olfactory epithelial thickness were collected for each cat. Statistical analysis was performed using a two-tailed paired t-test to compare means between groups.

Calcium imaging

For calcium imaging and electrophysiology studies, the nasal turbinates and septum were excised immediately post-mortem and placed into ice-cold Ringer's solution from a total of 42 cats (see Table 1). The epithelial tissue was dissected from the underlying turbinate and septal bones. Olfactory neurons were isolated by mincing the tissue with dissecting scissors, incubating the tissue in an "isolation solution" supplemented with 6 U/ml papain and 2 mM L-cysteine for 20 min. The tissue was then triturated and filtered through a nylon mesh into a "stop solution" (see below). For electrophysiological preparations, this suspension was applied to a Percoll (GE healthcare) gradient (Lischka et al., 1999) and a semi-purified suspension of olfactory neurons recovered for subsequent study. Recovered cells were then spread over concanavalin A–coated glass coverslips (22 × 60 cm, No. 0, Thomas Scientific Co.).

Intracellular calcium levels were monitored in freshly dissociated ORNs as described previously (Gomez et al. 2005). Briefly, cells were loaded with fura-2 AM by incubating the cells in the stop solution for at least one hour. Coverslips with fura-2-loaded cells were then situated in a recording chamber on the imaging setup. Cells were illuminated with UV light alternately at 340 and 380 nm (shuttered at 50–100 ms) to obtain ratiometric images. Emitted light from the fura-2 in the cells under 400× magnification was filtered at 510 nm and recorded with cooled CCD camera (Olympix, Perkin Elmer Life Sciences, Bethesda MD). Images were digitized using a Merlin Imaging Workstation (Perkin Elmer Life Sciences, Bethesda MD); intracellular calcium concentration ($[Ca^{+2}]_i$) was computed from the ratio of emitted light from 340/380 nm. Under these conditions, cells remained viable in the recording setup for over two hours.

Cells were continuously bathed with a Ringer's solution. Stimuli and pharmacological agents were applied and removed via superfusion. Mammalian Ringer's solution contained (in mM) 145 NaCl, 5 KCl, 1 $CaCl_2$, 1 $MgCl_2$, 1 Na pyruvate, and 20 Na-N-(2-hydroxyethyl) piperazine-N′-2-ethanesulfonic acid (Na HEPES). For High K^+ stimulation, 135 mM of NaCl was replaced with KCl. All compounds were obtained from Sigma Chemical Co. (St. Louis, MO). Odorants were obtained from Firmenich (Geneva, Switzerland) and from the Shiseido and Takasago Corporations (Tokyo, Japan). Mix A contained citralva, citronellal, eugenol, geraniol, hedione, menthone, and phenethylalcohol while Mix B contained ethyl vanillin, isovaleric acid, lilial, lyral, phenylethylamine, and triethylamine. The concentration of each odorant was 100 μM to make the study compatible with previous studies on feline, rat, and human ORNs using identical techniques. Odorants were dissolved directly in Ringer's by several rounds of vigorous vortexing and sonication. Pharmacological agents used were 3-isobutyl-1-methylxanthine (IBMX, 1 mM, Sigma-Aldrich, St. Louis, MO) and forskolin (20 μM, Calbiochem, San Diego, CA). Agents were dissolved in appropriate buffers and used at the concentrations indicated.

For the isolation solution, $CaCl_2$ and $MgCl_2$ from the mammalian Ringer's were replaced with 2 mM ethylenediaminetetraacetic acid (EDTA). The stop solution contained (in mM) 145 NaCl, 5 KCl, 2 $CaCl_2$, 1 $MgCl_2$, 5 D-glucose, 1 Na pyruvate, and 20 Na HEPES, supplemented with 8 μM fura-2/AM and 80 μg/ml pluronic F127 (Molecular Probes Inc., Eugene, OR).

Measurement of odorant responses

We measured average cellular calcium levels over the cell body and dendrite. $[Ca^{2+}]_i$ changes in the ORN dendrite and soma are important because they affect ORN function, therefore, playing a crucial role in signal transduction in ORNs (for review see (Schild and Restrepo, 1998). Responses were determined as described previously (Gomez et al., 2005),

based on onset and offset time course and magnitude relative to baseline level and signal noise.

Cell viability was assessed by monitoring physical appearance of the ORN and the baseline $[Ca^{2+}]_i$; viable cells were tested with odorants, and high K^+ depolarization which leads to a rise in $[Ca^{2+}]_i$ due to voltage-gated calcium channel activation that is observed in the majority of ORNs from felines (Gomez et al. 2005) and rodents (Tareilus et al., 1995). The responsive ORNs tested in this study exhibited odorant-elicited calcium responses similar to those seen previously (Gomez et al. 2005). In addition, two pharmacological agents were used to assess ORN function; forskolin and 3-isobutyl-1-methylxanthine (IBMX). These agents activate the canonical signal transduction pathway exhibited by the majority of mammalian ORNs by elevating cAMP levels (for review see Schild and Restrepo 1998). Forskolin (an adenylyl cyclase activator) leads to the production of cAMP and IBMX (a phosphodiesterase inhibitor) prevents breakdown of cAMP that is continuously produced by ORNs (Lowe and Gold 1995). Both should lead to a cAMP-mediated rise in $[Ca^{2+}]_i$ via the cyclic nucleotide gated channel and have been found to be effective in feline ORNs (Gomez et al., 2005). As the cellular response to IBMX depends on a certain basal level of cAMP production (which varies from cell to cell), it is typically observed in fewer cells, compared to forskolin.

To account for the possibility of within-subject correlations, between group comparisons of calcium response data were analyzed with the Genmod procedure in SAS (Cary, NC), which applies a Generalized Estimating Equations (GEE) method (Allison, 1999). A binomial distribution was specified using a logit link function and an exchangeable correlation structure. Subsequently, ad hoc pair-wise comparisons were made using the Chi-square statistic.

Electrophysiology

Olfactory cells were enzymatically dissociated, adhered to coated glass coverslips (above), and mounted in a recording chamber clamped onto the stage of an inverted Nikon microscope. Cells were continuously superfused with physiological Ringer's solution, via a gravity driven system with the outflow connected to a vacuum line.

Current and voltage signals were recorded using an Axopatch 200A amplifier (Axon Instruments) and saved to computer hard drive (2 kHz 4-pole Bessel, 10 kHz sampling rate for voltage gated currents), using a Digidata 1200 interface and Pentium computer running pCLAMP8 software. Pulse protocols were also generated by this system. An electronically controlled motorized micromanipulator (MP-285, Sutter instruments) was used to position the recording electrode.

Recordings were performed under perforated patch conditions, using 240 μg/ml Gramicidin (dissolved in DMSO) as an ionophore. Detailed methods are in Lischka et al. (1999). Briefly, borosilicate pipettes were pulled and fire-polished to a final resistance of 3–8 MΩ when filled with pseudointracellular solution. The tips of the pipettes were filled with filtered pseudointracellular solution and then backfilled with an intracellular solution supplemented with gramicidin. Once a GΩ seal was obtained, the capacitative artifacts resulting from application of small voltage pulses were monitored until low resistance access to the cell interior was obtained. Access resistance generally reached a steady level of 5–20 MΩ within 5–15 min. This technique resulted in long lasting, stable recordings (up to 1 hr or longer). Conventional voltage protocols, in combination with channel blockers and ion substitutions, were used to identify voltage-dependent conductances. The following solutions were used: Mammalian Ringer's (described above); pipette solution (in mM): 110 K-aspartate, 36 KCl, 1 $CaCl_2$, 1 $MgCl_2$, 10 HEPES. The pH was adjusted to 7.2 with the

hydroxide of the main cation and osmolarity was 310 mOsmol. Note that unbuffered calcium in the internal solution was used to ensure recording under perforated patch conditions. Rupture of the membrane patch under the pipette resulted in a rapid influx of calcium and termination of recording.

RESULTS

Nasal anatomy in control and MPS-affected cats

Figure 1A illustrates the complexity of the cat nasal cavity with the inserts showing the representative areas of interest for measuring the olfactory epithelial thickness (Fig 1B) and percent area occupied by goblet cells (Fig 1C). Unlike the rodent nasal cavity, the septal arch is localized more ventrally from the top of the skull. More caudally, the dorsal sinuses are prominent and extend dorsally beyond the cribriform plate, which results in localization of the olfactory bulbs below the sinuses.

Lysosomal storage was evident in chondrocytes in the nasal septum in sections from affected animals, based on the presence of abundant clear cytoplasm (Fig 1 D&E). The degree of storage increased with age and was obvious in MPS-affected adults (Fig 1 D, 88 weeks; Fig 1 E, 110 weeks) while no evidence for storage was found in tissue from older control animals (Fig 1 F, 288 weeks). In contrast, storage vesicles or vacuoles were not observable in cells within the olfactory epithelium of affected animals.

OE Morphology is altered in MPS

Goblet cell density was not significantly different between the three groups with 18.1% ± 5.89, 20.8% ± 5.7 and 24.4% ± 10.7 (mean ± SD) for MPS I, MPS VI, and controls, respectively (Fig 1G). We compared the thickness of the sensory epithelium among control and affected animals as a measure of general health of the tissue. The OE of MPS I cats was significantly thinner (49.7 μm ± 3.9, mean ± SD) than that of controls (73.2 μm ± 13.6; $t = 3.31$, $p<0.01$). The OE of MPS VI cats was intermediate in thickness (54.0 μm ± 9.0) and also significantly thinner than that of controls ($t=2.69$, $p<0.025$) but was not significantly different from MPS I (Fig 1H).

Immunohistochemistry

The decreased thickness of the sensory epithelium in both MPS I and MPS VI animals suggested an impact of MPS disease on ORNs. We evaluated the presence and morphology of ORNs via immunohistochemistry with specific antibodies against markers of mature ORNs (OMP) and general neuronal cell markers (NCAM and NST). OMP-labeled neurons showed the typical bipolar morphology of mature ORNs with an apical dendrite and olfactory knob and an axon on the basal end of the cell soma, fasciculating with other axons to form nerve bundles. OMP-labeled mature ORNs were detected in the sensory regions of the olfactory epithelium of control (Fig 2A&B) as well as MPS I (Fig 2C) and MPS VI (Fig 2D) cats. Cell bodies of OMP-positive cells in control tissue were lined up in the middle region of the epithelium (Fig 2B), while the cells in MPS I cats were less well organized (Fig 2C). OMP-positive cells were also more dispersed in MPS VI animals compared to controls and could be found closer to the basement membrane (Fig 2D). NST clearly immunolabeled neuronal cells in all three groups (Fig 2E–H). NST-positive cell bodies are localized in deeper layers of the epithelium, close to the basement membrane. NST also labeled nerve bundles intensely (shown for control tissue in Fig 2E). NCAM antibody also labeled ORNs in the sensory portion of the epithelium of normal controls (Fig 2I&J), as well as in MPS I- (Fig 2K) and MPS VI- (Fig 2L) affected cats. The antibodies labeled cells selectively, as non-sensory (respiratory) epithelium (Fig 2A, E&I) and negative controls (non-immune serum substitution of primary antibody (data not shown)) remained unstained.

Although the structural integrity of the sensory epithelium in affected cats appeared somewhat disorganized (localization of OMP-positive cell bodies, projection of olfactory dendrites to the mucosal surface), immunostaining verified the presence of ORNs in the sensory portions of the olfactory epithelium in both groups of MPS-affected animals.

ORN responses to odorants are impaired in MPS I

Next, we utilized cell physiological methods to determine whether ORN function in cats genotyped as homozygous for the MPS I or VI defect and controls from the same lines (see Table 1). ORNs were easily discerned based on their unique morphology: a round cell body, dendrite, and terminal knob (Gomez et al. 2005). There was no significant difference in the number of neurons from which we could obtain data for the MPS I-affected animals versus the control group (Table 1). The MPS VI cats yielded far fewer neurons compared to controls or MPS I-affected cats (Table 1). Based on our previous work (Gomez et al., 2005), we have found no age- or sex-related differences in feline olfactory neuron function, and so the data were pooled for each group.

No significant group effects were found for the frequency of responses to high K^+ and IBMX, indicating that the basic neurophysiological properties of ORNs from MPS I and VI cats were generally normal. In contrast, there was a significant group effect for responses to odors, with ORNs from MPS I cats exhibiting a marked deficit in odor responsiveness ($p = 0.006$). When tested with high K^+, 49% of cells from MPS I cats responded with $[Ca^{2+}]_i$ increases (Fig 3A&D), compared with 74% of ORNs from control cats (Fig 3C&D).

Forskolin and/or IBMX elicited $[Ca^{2+}]_i$ increases in ORNs from both MPS I and control cats (Fig 3A, C&D). When tested with IBMX, apparently fewer ORNs (11.5%) from MPS I cats showed a $[Ca^{2+}]_i$ change compared to ORNs from control cats (24%), but this difference was not significant (χ^2, $p = 0.458$). In spite of these normal functional properties, when tested with odorant Mix A or B, only 1% (1 out of 88) of ORNs from MPS I cats responded to odorant stimulation, while 26% of cells from control cats in this study responded to these odors (χ^2, $p = 0.0001$). This value is similar to that observed in a previous study of ORNs from a larger population of healthy cats (29%; (Gomez et al., 2005).

These functional differences appear to be specific for MPS I. The low frequency of viable neurons that we could record from MPS VI cats makes direct statistical comparisons with MPS I difficult. However, 64% of cells tested responded to high K^+ and 8 out of 16 cells responded to Mix A or B (Fig 3B&D); these cells also responded to forskolin and IBMX. Thus, while MPS VI may alter cell viability during dissociation, the impairment in odorant responsiveness appears to be specific to MPS I-affected animals.

Electrophysiological properties of ORNs

To test whether the functional deficits in ORNs from MPS I cats are caused by deficits in cellular components that maintain the basic electrical properties of the neurons, we performed perforated patch recordings on ORNs from control (n = 101) and MPS I-affected cats (n = 10). In the calcium imaging experiments described above, only a small number of viable ORNs could be isolated from MPS VI-affected animals. The cells that were obtained showed normal responses to the applied stimuli. Therefore, no attempt was made to perform electrophysiological experiments on isolated ORNs from MPS VI animals. As no prior studies of the electrophysiological properties of ORNs from cats have been reported, we examined an array of basic voltage-sensitive conductances known to be present in ORNs of other mammals. ORNs from MPS I animals had an average resting membrane potential of −68 mV ±3 mV (mean ±SEM; n=2), similar to that of cells from control cats: −64 mV ±5 mV (n=16). Figure 4A shows an example of a family of currents elicited by voltage steps

from −100mV to +80mV in normal cats. Several voltage-activated currents could be discerned: a fast transient inward current, a transient outward current and a sustained outward current. Similar currents were elicited in ORNs isolated from MPS I-affected cats (Fig. 4B). Subsequently, several voltage-activated conductances were analyzed in more detail. Two types of voltage-activated outward potassium currents were observed in both groups: a transient or "A" type current that was blocked by pre-pulse inactivation (data not shown) and a sustained delayed rectifier potassium current that was greatly reduced by 20 mM TEA^+ in the bath solution or replacement of K^+ with Cs^+ in the pipette solution (data not shown). The peak outward current for control cells was 842 pA ± 74 pA (n = 100) and for ORNs from MPS I animals was 830 pA ± 372 pA (n = 5). A majority of ORNs (74% or 75/101 for control and 67% or 6/9 for MPS I-affected) possessed an inward rectifier current that was elicited by hyperpolarizing steps from −80 mV and was blocked by 10 mM Ba^{2+} in the bath solution.

The voltage-activated sodium current is crucial for the excitability of ORNs and neurons in general, being responsible for the depolarizing phase of an action potential. 69% (70 of 101) of recorded ORNs from control animals had a sodium current with an average amplitude of 257 pA ± 28 pA (n = 64). Sodium currents of comparable amplitude (320 pA ± 176 pA) were observed in 90% (9 of 10) of ORNs from MPS I cats. The sodium currents were completely blocked by bath application of 200 nM tetrodotoxin (TTX) in controls (n = 6) and MPS I (n = 2). For a more detailed comparison, the characteristic kinetics of the sodium conductance were analyzed (Fig 5). Current activation (Fig 5A–C), pre-pulse inactivation (Fig 5D–F), and the time for recovery from inactivation (Fig 5G–I) were not significantly different in these cells. These data suggest that MPS I disease does not broadly prevent expression of basic neurophysiological properties.

ORNs also possess voltage-activated calcium currents that allow the influx of calcium upon depolarization of the cell membrane. The reduced response frequency to high potassium application in MPS I animals observed in the calcium imaging experiments suggested a possible dysfunction in these channels. We were only able to test once for voltage-activated calcium currents in MPS I cats (Fig 6A–E). After the outward current was reduced with 20 mM TEA^+ and the sodium current blocked with 200 nM TTX (Fig 6B), 10 mM Ba^{2+} was washed in to enhance the calcium current (Fig 6C). Two apparent inward current components were elicited: a fast transient and a sustained current. The fast component was not carried by sodium channels, as TTX was still present and it had blocked the sodium current completely (Fig 6B). The L-type calcium channel blocker nimodipine (10 μM) reduced both current components greatly (by 81% for the sustained current) (Fig 6D&E). Two Ba^{2+}-enhanced calcium current components were also found in a cell from a control animal under similar conditions (Fig 6F) while the majority of cells tested only displayed a sustained current (7 of 8). This demonstrated that ORNs from MPS I-affected cats possess calcium currents similar to those found in controls.

DISCUSSION

Our studies have revealed intriguing differences in the anatomy of the olfactory system in these affected cats: the sensory olfactory epithelium was significantly thinner and its structural integrity abnormal. In addition, functional properties of ORNs from cats with MPS I were compromised: while ORNs from MPS I cats displayed normal electrical properties, these cells failed to respond to odorant stimuli. This finding suggests a dysfunction in odorant receptor and GTP-binding regulatory protein activity or coupling - events that are upstream of adenylyl cyclase III, and cyclic nucleotide-gated channels in the transduction cascade. The physiological impairments appeared to be specific for MPS I:

ORNs from MPS VI-affected cats, although less prevalent, functioned more like their normal counterparts.

As olfactory sensory neurons are replaced throughout life from a population of resident progenitor cells within the epithelium, the thickness and integrity of the sensory epithelium has been used as a general indicator of the health of the OE after infection (Ge et al., 2002) or removal of the olfactory bulbs (Booth et al., 1981; Constanzo & Graziadei, 1983). Accordingly, the abnormal OE seen in both MPS I and VI suggests the involvement of GAGs in development and maintenance of the integrity of the olfactory neuroepithelium. Heparan sulfate proteoglycans are known to play an important role in neural development and neuronal differentiation (Chipperfield et al., 2002). Accordingly, a reduction in OE thickness may be due to an effect on the genesis, maturation, or function of the ORNs. Transgenic models impairing development of the OE such as the mash 1−/− mouse, exhibit fewer mature ORNs and thinner OE (Cau et al., 2002). While we did not examine proliferation, two aspects of our data argue against a gross defect in neurogenesis or neuronal maturation: the persistence of immunostaining for general neuronal markers and OMP, and the presence of morphologically normal mature ORNs, based on the presence of a distinct dendrite, knob, and cilia, in dissociated cells from affected cats.

Interfering with ORN function can also lead to OE thinning. Under these conditions, mature neurons are generated, but their lifespan is reduced and the rate of neuronal replacement fails to maintain normal mature neuronal populations. Nares occlusion (Farbman et al., 1988; Suh et al., 2006) or transgenic manipulation of the signaling cascade (Baker et al., 1999) interfere with ORN function and result in OE thinning. Similarly, the lack of odor sensitivity in MPS I ORNs may contribute to the OE thinning, although this would not appear to account for the effect in MPS VI.

Our studies did not attempt to examine the specific changes in the cellular profile of the OE that might account for the observed differences in OE thickness, in part due to the lack of antibody cross-reactivity in feline tissue for classical markers of OE cell types. Thus, it is possible that epithelial thickness differences are due to differences in other elements of the OE, or to differences in extracellular matrix that influence tissue compression during processing. Consistent with the immunocytochemical pattern, we did not detect a difference in the prevalence of mature ORNs in dissociated OE preparations based on the presence of a morphologically distinct dendrite, knob, and cilia in tissue from MPS I-affected cats. The lower prevalence of morphologically distinct ORNs in the MPS VI-affected cats could be due to fewer mature cells in the tissue, but the immunohistochemical results, although qualitative, argue against this. Alternatively, differences in the ability of the cells to withstand dissociation, possibly due to differences in extracellular matrix composition, could account for the low number of ORNs detected in the dissociated OE preparations from MPS VI-affected animals. Overall, these results suggest that neurogenesis itself is not impaired by these disorders, but that maintenance of the structural integrity of the OE is affected in both MPS I and MPS VI. Alternatively, or in addition, the abnormal GAG concentration or turnover may influence early developmental processes that impact on the progenitor cells or their competence to progress through the normal lineage.

As the more severe forms of MPS I, but not MPS VI, are associated with mental retardation, the physiological deficits specific to MPS I suggest a specific mechanism that may underlie MPS I-associated neurological dysfunction. Odorant signaling begins with odorants binding to G-protein coupled receptors to activate second messenger synthesizing enzymes, leading to increases in intracellular second messenger concentrations, the opening of cation channels, and subsequent depolarization and associated calcium fluxes (Schild and Restrepo, 1998). These basic properties are generally similar among all mammals studied, and the data

we present here are consistent with earlier functional studies of cat ORNs (Gomez et al., 2005). Pharmacological manipulations during calcium imaging experiments suggest that second messenger-producing enzymes and calcium flux mechanisms are functional in MPS I-affected cats. The electrophysiological results indicate that ORNs from cats exhibit the same complement of voltage-activated ion currents found in ORNs from other species studied (Schild and Restrepo, 1998), and that these currents are comparable in MPS I-affected cats. Thus, the functional deficits that were observed in the calcium flux experiments were apparently due to impairments in signaling components, related to second messenger-mediated signal transduction cascades.

The most parsimonious explanation for the lack of odorant sensitivity in these cats would be that the G-protein-coupled receptors are inappropriately tagged for traffic to the cell membrane. Functional expression of these receptors involves post-translational processing in the endoplasmatic reticulum and Golgi apparatus (Gimelbrant et al., 2001); the last stages of this process involve enzymatic modification of carbohydrate residues important for membrane trafficking and insertion. This process is common to numerous G-protein-coupled receptors within the CNS. Thus, failure of these receptors to properly insert into the neuronal cell membrane and/or to couple to their associated signaling pathways may represent a key general mechanism underlying neurological dysfunction in MPS I. These are the first data to our knowledge to suggest a specific neurophysiological defect underlying MPS I-associated mental retardation. If such a general receptor processing impairment occurs, efforts aimed at early therapeutic intervention, prior to the onset of cognitively discernible mental impairment, become of even greater importance.

Supplementary Material

Refer to Web version on PubMed Central for supplementary material.

Acknowledgments

Support information: Funded by grants from the National Science Foundation DBI-021631010B0517748 (N.E.R.) and Monell Chemical Senses Center and NIH DK25759 and RR02512 (MH).

We would like to thank Patricia O'Donnell, Meg Weil, Karyn Cullen, Mike Kurnellas, and Tatyana Dankulich for their valuable technical assistance. We thank our summer students Olivera Crenshaw, Rena Griggs, Daniel Montiel and Natasha Rivers for their dedicated work on parts of the histological aspects of this study. Johannes Reisert and John Teeter generously provided helpful advice and discussion.

Literature cited

Allison, PD. Logistic Regression Using the SAS System: Theory and Application. Cary, NC: SAS Institute Inc.; 1999. p. 304

Baker H, Cummings DM, Munger SD, Margolis JW, Franzen L, Reed RR, Margolis FL. Targeted deletion of a cyclic nucleotide-gated channel subunit (OCNC1): biochemical and morphological consequences in adult mice. J Neurosci. 1999; 19:9313–9321. [PubMed: 10531436]

Booth WD, Baldwin BA, Poynder TM, Bannister LH, Gower DB. Degeneration and regeneration of the olfactory epithelium after olfactory bulb ablation in the pig: a morphological and electrophysiological study. Q J Exp Physiol. 1981; 66:533–540. [PubMed: 6914685]

Buiakova OI, Krishna NS, Getchell TV, Margolis FL. Human and rodent OMP genes: conservation of structural and regulatory motifs and cellular localization. Genomics. 1994; 20:452–462. [PubMed: 8034318]

Cau E, Casarosa S, Guillemot F. Mash1 and Ngn1 control distinct steps of determination and differentiation in the olfactory sensory neuron lineage. Development. 2002; 128:1871–1880. [PubMed: 11934853]

Chipperfield H, Bedi KS, Cool SM, Nurcombe V. Heparan sulfates isolated from adult neural progenitor cells can direct phenotypic maturation. Int J Dev Biol. 2002; 46:661–670. [PubMed: 12141455]

Costanzo RM, Graziadei PPC. A quantitative analysis of changes in the olfactory epithelium following bulbectomy in hamster. The Journal of Comparative Neurology. 1983; 215:370–381. [PubMed: 6863590]

Farbman AI, Brunjes PC, Rentfro L, Michas J, Ritz S. The effect of unilateral naris occlusion on cell dynamics in the developing rat olfactory epithelium. J Neurosci. 1988; 8:3290–3295. [PubMed: 2459323]

Ferrando S, Bottaro M, Gallus L, Girosi L, Vacchi M, Tagliafierro G. First detection of olfactory marker protein (OMP) immunoreactivity in the olfactory epithelium of a cartilaginous fish. Neurosci Lett. 2007; 413:173–176. [PubMed: 17174032]

Ge Y, Tsukatani T, Nishimura T, Furukawa M, Miwa T. Cell death of olfactory receptor neurons in a rat with nasosinusitis infected artificially with *Staphylococcus*. Chem Senses. 2002; 27:521–527. [PubMed: 12142328]

Gimelbrant AA, Haley SL, McClintock TS. Olfactory receptor trafficking involves conserved regulatory steps. J Biol Chem. 2001; 276:7285–7290. [PubMed: 11060288]

Gomez G, Lischka FW, Haskins ME, Rawson NE. Evidence for multiple calcium response mechanisms in mammalian olfactory receptor neurons. Chem Senses. 2005; 30:317–326. [PubMed: 15800218]

Hahn CG, Gomez G, Restrepo D, Friedman E, Josiassen R, Pribitkin EA, Lowry LD, Gallop RJ, Rawson NE. Aberrant intracellular calcium signaling in olfactory neurons from patients with bipolar disorder. Am J Psychiatry. 2005; 162:616–618. [PubMed: 15741484]

Haskins ME. Animal models for mucopolysaccharidosis disorders and their clinical relevance. Acta Paediatrica Suppl. 2007; 96:56–62.

Haskins ME, Aguirre GD, Jezyk PF, Patterson DF. The pathology of the feline model of mucopolysaccharidosis VI. Am J Pathol. 1980; 101:657–674. [PubMed: 6778219]

Katada S, Tanaka M, Touhara K. Structural determinants for membrane trafficking and G protein selectivity of a mouse olfactory receptor. J Neurochem. 2004; 90:1453–1463. [PubMed: 15341529]

Keller A, Margolis FL. Immunological studies of the rat olfactory marker protein. J Neurochem. 1975; 24:1101–1106. [PubMed: 805214]

Lee MK, Rebhun LI, Frankfurter A. Posttranslational modification of class III β-tubulin. Proc Natl Acad Sci. 1990a; 87:7195–7199. [PubMed: 2402501]

Lee MK, Tuttle JB, Rebhun LI, Cleveland DW, Frankurter A. The expression of posttranslational modification of a neuron-specific β-tubulin isotype during chick embryogenesis. Cell Motil Cytoskeleton. 1990b; 17:118–132. [PubMed: 2257630]

Lischka FW, Teeter JH, Restrepo D. Odorants suppress a voltage-activated K^+ conductance in rat olfactory neurons. J Neurophysiol. 1999; 82:226–236. [PubMed: 10400951]

Lovell MA, Jafek BW, Moran DT, Rowley JC 3rd. Biopsy of human olfactory mucosa. An instrument and a technique. Arch Otolaryngol. 1982; 108:247–249. [PubMed: 7073597]

Lowe G, Gold G. Olfactory transduction is intrinsically noisy. Proc Natl Acad Sci U S A. 1995; 92:7864–7868. [PubMed: 7544007]

Naegele JR, Barnstable CJ. A carbohydrate epitope defined by monoclonal antibody VC1.1 is found on N-CAM and other cell adhesion molecules. Brain Res. 1991; 559:118–129. [PubMed: 1723642]

Neill JM, Barnstable CJ. Expression of the cell surface antigens RET-PE2 and N-CAM by rat retinal pigment epithelial cells during development and in tissue culture. Exp Eye Res. 1990; 51:575–583.

Neufeld, EF.; Muenzer, EJ. The Mucopolysaccharidoses. In: Scriver, CR., editor. The metabolic & molecular bases of inherited disease. New York: McGraw-Hill; 2001. p. 2465-2494.

Ronnett GV, Leopold D, Cai X, Hoffbuhr KC, Moses L, Hoffman EP, Naidu S. Olfactory biopsies demonstrate a defect in neuronal development in Rett's syndrome. Ann Neurol. 2003; 54:206–218. [PubMed: 12891673]

Roskams AJI, CAI X, Ronnet GV. Expression of neuron-specific beta-III tubulin during olfactory neurogenesis in the embryonic and adult rat. Neuroscience. 1998; 83:191–200. [PubMed: 9466409]

Sambrook, J.; Fritsch, EF.; Maniatis, T. Molecular Cloning: A Laboratory Manual. 2. Cold Spring Harbor Laboratory Press; Cold Spring Harbor, NY: 1989.

Schild D, Restrepo D. Transduction mechanisms in vertebrate olfactory receptor cells. Physiol Rev. 1998; 78:429–466. [PubMed: 9562035]

Suh KS, Kim SY, Bae YC, Ronnett GV, Moon C. Effects of unilateral naris occlusion on the olfactory epithelium of adult mice. NeuroReport. 2006; 17:1139–1142. [PubMed: 16837842]

Tareilus E, Noe J, Breer H. Calcium signals in olfactory neurons. Biochim Biophys Acta. 1995; 1269:129–138. [PubMed: 7488645]

Tisay KT, Key B. The extracellular matrix modulates olfactory neurite outgrowth on ensheathing cells. J Neurosci. 1999; 19:9890–9899. [PubMed: 10559398]

Toba Y, Horie M, Sango K, Tokashiki A, Matsui F, Oohira A, Kawano H. Expression and immunohistochemical localization of heparan sulphate proteoglycan N-syndecan in the migratory pathway from the rat olfactory placode. Eur J Neurosci. 2002; 15:1461–1473. [PubMed: 12028356]

Walkley SU, Haskins ME, Shull RM. Alteration in neuron morphology in mucopolysaccharidosis type I. A Golgi study. Acta Neuropathol. 1988; 75:611–620. [PubMed: 2454013]

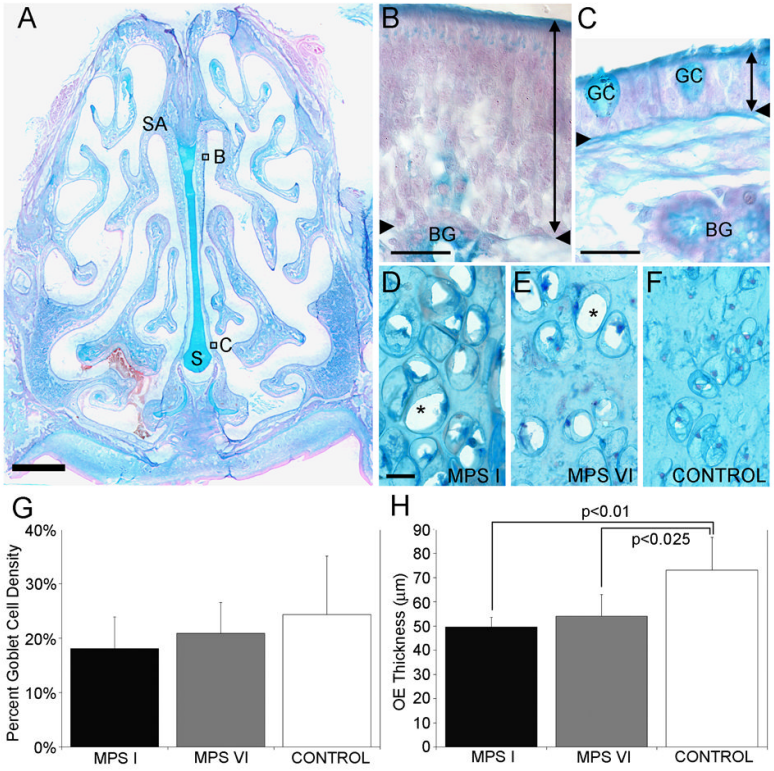

Figure 1.

Anatomy and morphometry of the OE in MPS-affected and control cats. A. A coronal cross-section of a control cat stained with alcian blue and nuclear fast red. The ventral aspect of the septal arch (SA) is lined with sensory OE, whereas the base of the septum (S) is lined with respiratory epithelium. Scale bar = 2mm. B. Higher magnification of the sensory OE consisting of supporting cells, ORNs, basal cells and the duct of Bowman's glands (BG). The thickness of the OE was measured from the apical surface to the basement membrane (double-headed arrow line). The region of OE is indicated in Fig 1A. C. A higher magnification of the respiratory epithelium (double-headed arrow line) consisting of respiratory cells and goblet cells (GC). The region of respiratory epithelium is indicated in Fig 1A. D and E. In the nasal septum of affected MPS I and MPS VI animals, lysosomal storage was evident in chondrocytes, based on the presence of abundant clear vacuoles in the cytoplasm from which stored GAGs were lost during tissue processing (asterisks). F. In control animals, chondrocytes in the septum showed no evidence to lysosomal storage. G. The goblet cell density was not significantly different between MPS-affected and control cat RE. H. There were significant differences between the OE thickness of MPS I and control cats ($p<0.01$) and between MPS VI and control ($p<0.25$) cats. Mean ± standard deviation. Scale bars = 20 μm.

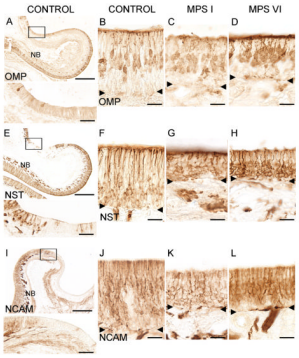

Figure 2.

Immunohistochemical localization of ORNs in control and affected cats. A. OMP-immunoreactivity (ir) of mature ORNs in a region of the ethmoturbinate in a control animal. Inset: a higher magnification of the boxed area shows individual labeled cells and no labeling of adjacent respiratory cells. B. OMP-ir cells project dendritic processes to the apical surface of the sensory epithelium with their cell bodies localized in the middle layers of the tissue. C. OMP-ir was detected in MPS I-affected animals. D. OMP-ir was detected in MPS VI-affected animals. E. NST-ir in olfactory epithelium of a control cat. Cells are labeled in the epithelium and NST-ir olfactory nerve bundles are seen below the basement membrane in the lamina propria. Inset: Higher magnification of NST-ir in ORNs. Left portion of the epithelium contains NST-positive cells while center portion shows non-sensory epithelium, which lacks NST-ir cells. F. NST-ir cell bodies tend to be found above the basement membrane and below the OMP positive cells (2B) suggesting that NST labeled more immature ORNs. Strong ir was also present in the dendrites and olfactory knobs. G. NST-ir ORNs were present in MPS I animals. H. NST-ir ORNs were also present in MPS VI animals. I. NCAM-ir in olfactory epithelium from a control cat. NCAM-ir (sensory) and NCAM negative (non-sensory) epithelium is visible. Note the pronounced labeling of nerve bundles below the sensory portion of epithelium (NB). Inset: Higher magnification of the transition area between sensory (left) and non-sensory epithelium (right) which is clearly demarcated by NCAM-ir. J. NCAM-labeled cells throughout the sensory part of the epithelium in control cats. K. NCAM –ir was detected in the epithelium of MPS I animals. L. NCAM-ir was detected in MPS VI animals. The reduced OE thickness in both MPS I and MPS VI animals can be seen in their respective images. NB = nerve bundles. Arrowheads = basement membrane. Scale bars are 250 μm for A, E, and I; 40 μm for the insets and 20 μm for B–D, F–H and J–L.

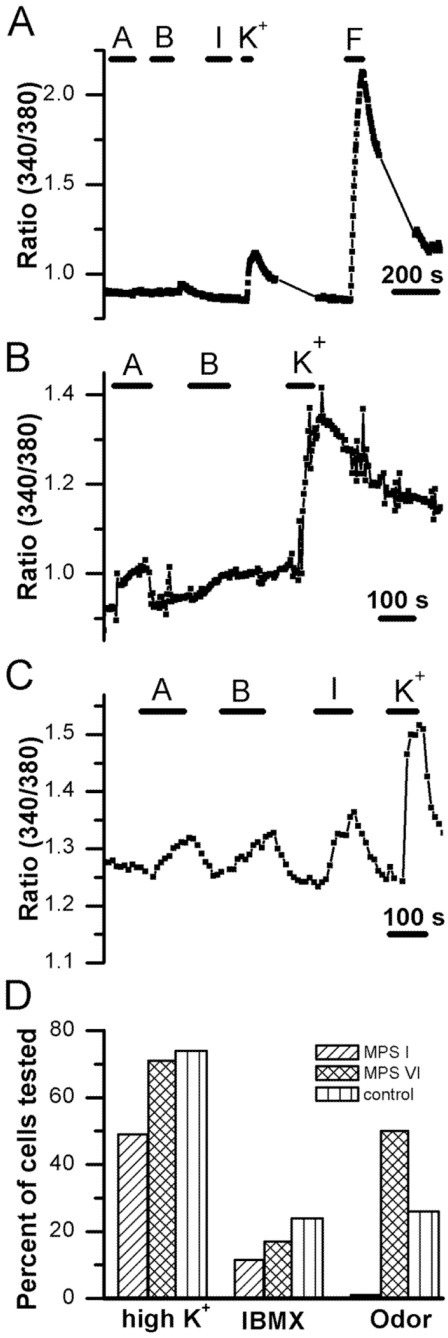

Figure 3.

Calcium imaging reveals differences in responsiveness to stimulation. A. Example of a trace showing fluorescence ratio values recorded from an ORN from an MPS I cat. The cell showed no $[Ca^{2+}]_i$ increase to two odor mixtures or IBMX but had a small response to application of high potassium solution and a large $[Ca^{2+}]_i$ increase to the adenylate cyclase activator forskolin. A = odorant mixture A; B = odorant mixture B, F = 20 μM forskolin; I = 1 mM 3-isobutyl-1-methylxanthine (IBMX); K^+ = 135 mM potassium Ringer. B. Recording of an ORN from an MPS VI-affected cat. This cell exhibited a response to odor mixture A and to high K^+ with no response to odor mixture B. C. Calcium levels increase in an ORN from a control animal in response to both odorant mixtures as well as to IBMX and to

depolarization with high K^+. D. Bar chart of response frequencies for the calcium responses to application of 135 mM potassium, IBMX, and odorant mixture A or B. Responsiveness to depolarization with high K^+ was similar between MPS VI cats and controls but was lower in MPS I animals. There was also a trend for fewer cells from affected cats, both MPS I and MPS VI, to respond to IBMX, although this difference was not significant when considering within-animal correlation (see methods). The response frequencies to odorant mixtures were significantly different among groups with only 1 of 88 cells from the MPS I animals responding.

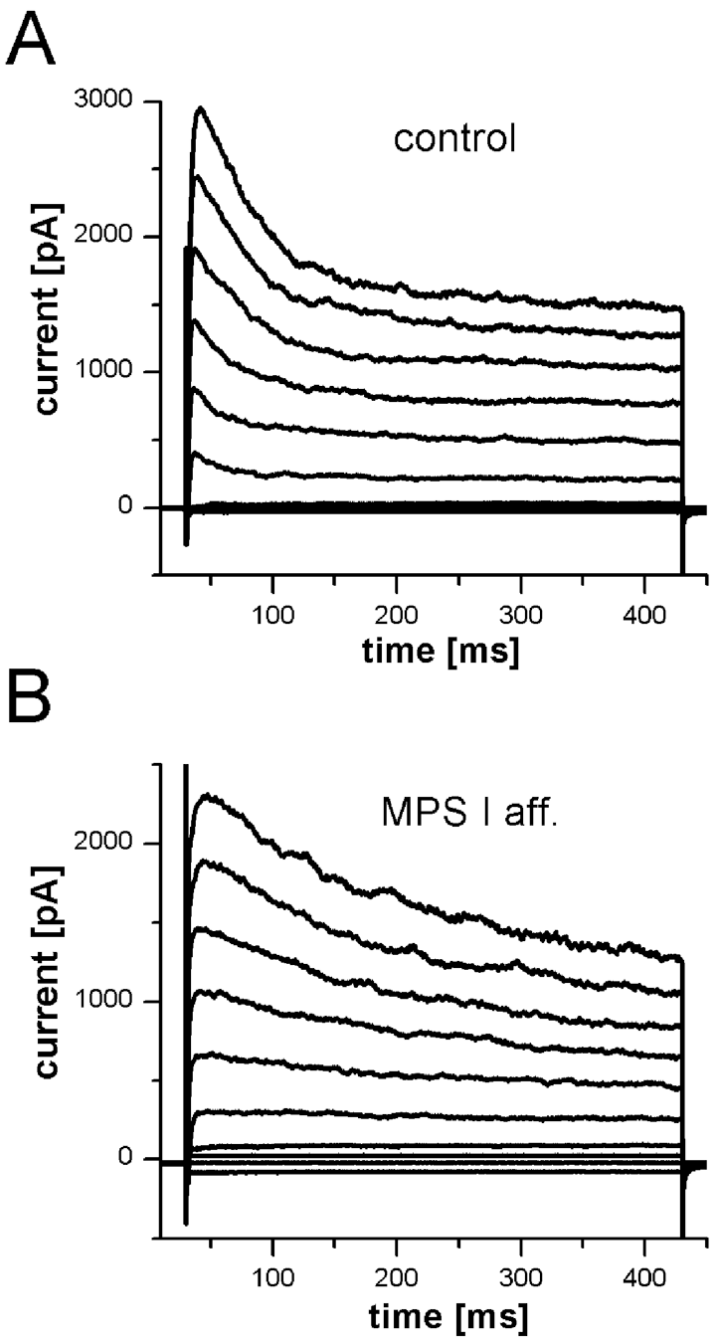

Figure 4.

Voltage-activated currents were present in ORNs from MPS I-affected and control cats. Currents were elicited by voltage steps from −100 mV in 20 mV increments to + 80 mV. Holding potential was −70 mV. A. In an ORN from a control cat, two outward current components (a transient and a sustained current) were observed, as well as a fast transient inward current. B. A recording from an ORN of an MPS I-affected cat showed similar currents with somewhat different time course but comparable amplitudes.

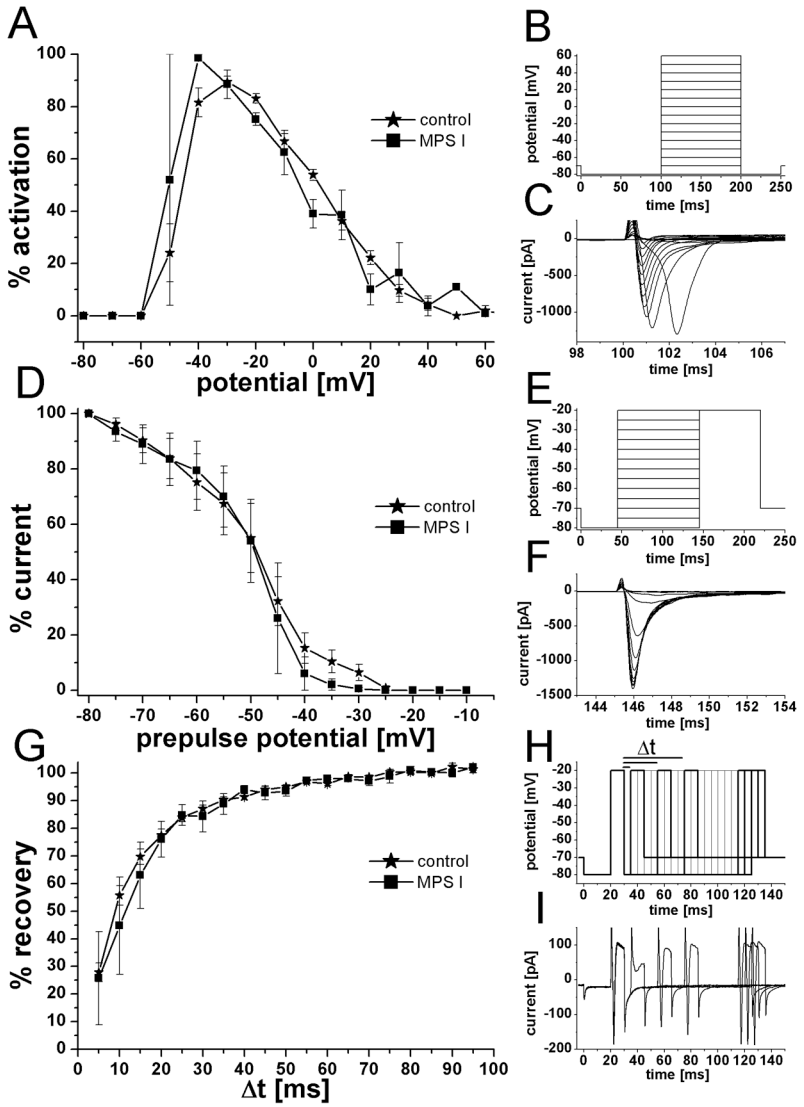

Figure 5.

Kinetics of voltage-activated sodium currents were similar in ORNs from MPS I-affected and control cats. A. Plot of sodium current activation vs. potential with the peak current for individual recordings set at 100% to normalize the data. B. Pulse protocol used to elicit sodium currents. Cells were held at −70 mV and, after a prepulse of −80 mV, the potential was stepped in 10 mV increments to +60 mV. C. Example of voltage-activated sodium current from a MPS I-affected ORN. The peak current was 1300 pA and was elicited at −40 mV. D. Plot of sodium current prepulse inactivation. Current amplitude of a test pulse after a prepulse potential of −80 mV was set a 100% to normalize the data. Half inactivation for the two groups was almost identical at −49 mV (−48.9 mV for control and −49.3 mV for MPS I). E. Pulse protocol for prepulse inactivation. Cells were held at −70 mV and briefly hyperpolarized to −80 mV. Prepulses were applied from −80 mV to +20 mV in 5 mV steps and the current amplitude was determined with a test pulse to +20 mV. F. Example of sodium currents elicited by the test pulse to + 20 mV; same ORN as in C. G. Recovery-from-inactivation plot showed no difference in recovery of the sodium current between the two groups. The amplitude of the current induced by a first voltage step was set as 100% and a second test pulse was applied with increasing time interval between the two. The %

amplitude of the second response compare to the first was plotted against the time between pulses (Δt). H. Pulse protocol to determine time to recovery from inactivation. Membrane potential was stepped twice from −80 mV to −20 mV for 10 ms each and the time between the two pulses was increased in 5 ms steps. Bolder lines correspond to current traces in I. I. Examples for current traces recorded from an MPS I ORN. Time interval between the pulses for the shown traces was 5 ms, 35 ms, 45 ms, 85 ms, 90 ms, and 95 ms. While the sodium current is largely reduced after 5 ms recovery time, it fully recovered with longer time intervals.

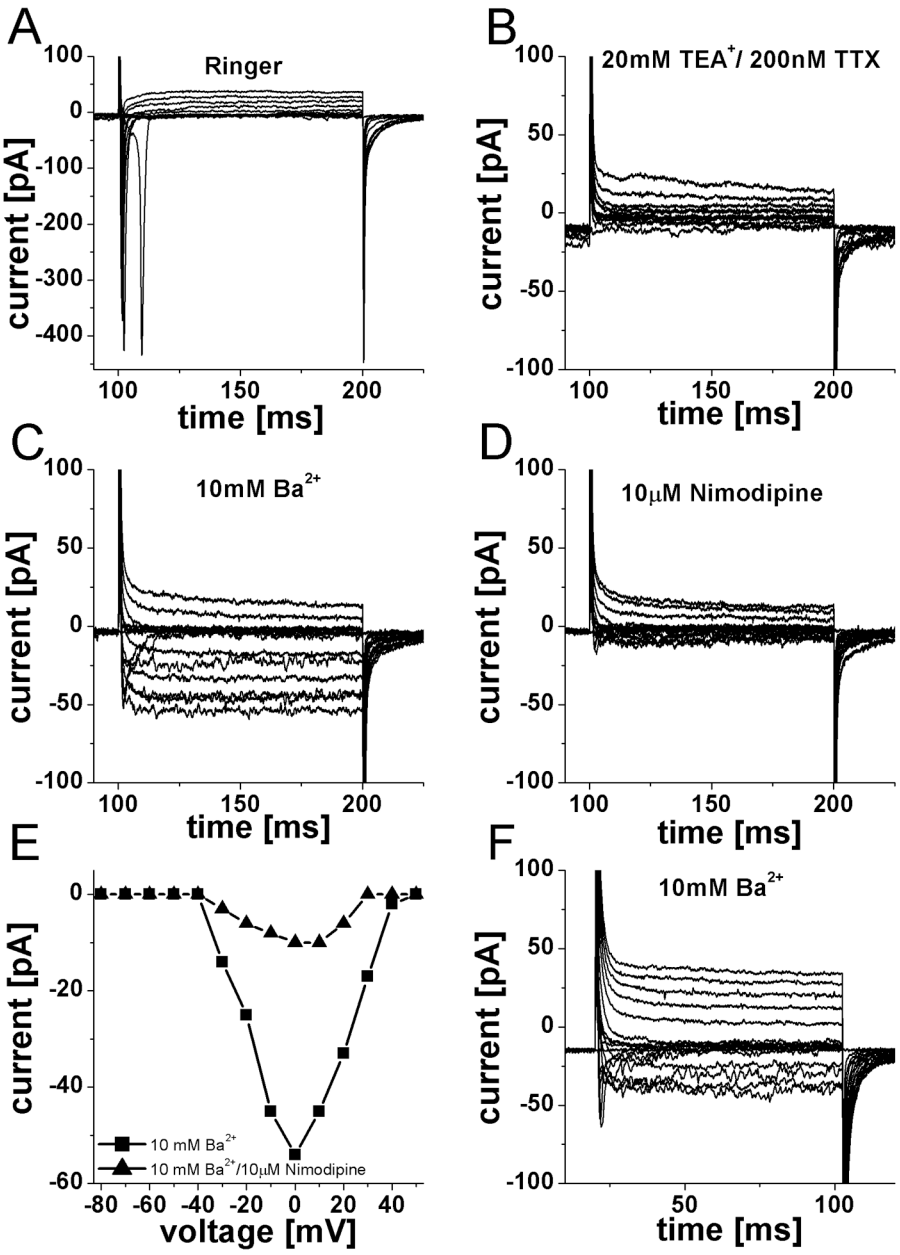

Figure 6.

Voltage-activated calcium currents were present in ORNs from both control and MPS I-affected cats. A. Family of current elicited by pulse protocol from Fig 5B, in Ringer solution, a fast sodium inward current was observed. B. Addition of 20 mM tetraethylammonium^{+} (TEA^{+}) and 200nM tetrodotoxin (TTX) reduced the outward currents and abolished the sodium current. C. Further addition of 10 mM Ba^{2+} enhanced voltage-activated calcium currents present in this cell. A fast, transient component as well as a sustained current is visible. D. Adding 10 μM Nimodipine (a potent L-type calcium channel blocker) greatly reduced both components of inward current. E. Current-voltage relationship for the sustained inward current in the presence of 10 mM Ba^{2+} and after addition of 10 μM nimodipine. Nimodipine reduced the current amplitude by 81%. F. Recording from an ORN

from a control cat under identical conditions as in C. Two inward current components of comparable size and time course were observed.

Table 1

Subject characteristics and cell yield for calcium imaging experiments

Experiments (n = 42)	# of cells tested (cells/experiment)	Age (average)
MPS I affected (n = 6)	88 (14.7)	2 months – 3.5 years (19 months)
MPS VI affected (n = 6)	16 (3.7)	2 weeks – 2 years (8 months)
Controls (n = 30)	304 (10.1)	2 weeks – 5 years (6 months)